Capacitance transient study of the metastable *M* center in *n*-type 4*H*-SiC

H. Kortegaard Nielsen* and A. Hallén
Solid State Electronics, Royal Institute of Technology, Electrum 229 SE-16440 Kista-Stockholm, Sweden

B. G. Svensson
Department of Physics, Physical Electronics, Oslo University, P. B. 1048 Blindern, N-0316 Oslo, Norway
(Received 20 April 2005; published 3 August 2005)

The metastable *M* center in *n*-type 4*H* silicon carbide is studied in detail after it has been introduced by 2.5 MeV proton irradiation with a fluence of 1×10^{12} cm^{-2}. The experimental procedures included deep-level transient spectroscopy, carrier capture coefficient and capacitance versus temperature measurements, and pulse-train measurements. The pulse-train measurements are reproduced by simulations. Three band-gap levels have previously been assigned to the *M* center: M_1 at $E_C-0.42$ eV, M_2 at $E_C-0.63$ eV, and M_3 at $E_C-0.83$ eV, where E_C is the conduction-band edge. Direct measurements of the majority-carrier capture cross sections show that the cross section values extracted from Arrhenius plots are about two orders of magnitude too large, indicating a large entropy factor. A detailed configuration diagram of the *M* center is presented, including charge state levels and reconfiguration barriers. Evidence in support of a fourth *M* center level, not explicitly observed, is presented. Isochronal and isothermal annealing experiments show that the *M* center anneal out between 310 and 370 °C in a process displaying first-order kinetics. The annealing process, which is shown to have an activation energy of 2.0 eV, is identified as dissociation.

DOI: 10.1103/PhysRevB.72.085208 PACS number(s): 71.55.−i, 61.72.Cc, 61.82.Fk

I. INTRODUCTION

Deep-level transient spectroscopy (DLTS) on electron- and proton-irradiated *n*-type 4*H* silicon carbide shows that many defect levels are generated by low-dose irradiation and that annealing at room temperature or slightly above (<300 °C) significantly changes the defect composition.[1–4] This low-dose and low-annealing temperature regime has often been neglected in other defect studies in SiC, even though this regime offers great opportunities for a fundamental understanding of point defects in silicon carbide. Most of the defects in silicon carbide have been neither studied in detail nor identified. In 4*H* silicon carbide, the *Z* defect is well known and has been studied because of its presence in as-grown as well as in irradiated material.[5] It appears at suitable temperatures for DLTS with the $Z_{1,2}(-/+)$ level positioned approximately 0.68 eV below the conduction-band edge E_C. The identity of the *Z* defect is still debated.[6–8] The two levels S_1 at $E_C-0.40$ eV and S_2 at $E_C-0.71$ eV originate from different charge states of the same defect[3,9,10] (the *S* center) and three other levels M_1, M_2, and M_3 have been assigned to a metastable defect (the *M* center).[11] Defect levels have also been observed deeper into the band gap, but these defects are inaccessible by DLTS in a low-temperature annealing study because probing these levels requires temperatures so high that the measurement itself would cause annealing.

Metastability of point defects have been reported earlier, e.g., for the carbon-carbon[12,13] and carbon–group-V-atom[14] pairs in silicon and for an unknown, tristable defect in 6*H* silicon carbide.[15] As described in Ref. 11, the *M* center in 4*H* silicon carbide has been observed in two configurations (*A* and *B*). The levels M_1 and M_3 belong to configuration *A* and M_2 to configuration *B*. It was also shown in Ref. 11 that there is a one-to-one correlation between the two configurations and that the configurtion of the *M* center can be changed reversibly. Configuration *A* is introduced at temperatures ≥20 °C only when reverse bias is applied so that the active DLTS region is depleted of charge carriers. In the depletion region, the *M* centers are thus prohibited from capturing electrons; and once they have become empty through emission of electrons, they will reconfigure from *B* to *A* through a thermally controlled process which has an energy barrier of 0.90 eV. The opposite transformation (*A* to *B*) requires temperatures ≥140 °C and filled *M* centers, which are obtained by applying zero bias voltage, so that the active DLTS region is no longer depleted. The energy barrier for the reconfiguration from *A* to *B* is 1.4 eV.

Here we report on the full annealing behavior of the *M* center, and furthermore, we present a configuration diagram based also on filling pulse measurements and simulations of capacitance measurements during capture-emission sequences. In addition to the three observed levels $M_{1,2,3}$, the data strongly suggest the existence of a fourth deep level, which we have labeled M_4. This level is observed indirectly when the *M* center is in configuration *B*.

II. EXPERIMENTAL PROCEDURE

A 20-μm-thick, nitrogen-doped layer was grown on a Cree substrate by chemical vapor deposition at Linköping University.[16] A doping concentration of $(1-2)\times10^{15}$ cm^{-3} was determined in the layer by capacitance-voltage measurements. High-quality Schottky diodes were prepared[17] by deposition of 1200 Å TiW followed by thermal annealing at 500 °C. Subsequently, the diodes were implanted with 2.5 MeV protons at the tandem accelerator at the Ångström Laboratory in Uppsala.[18] Several samples were implanted

with a fluence of 1×10^{12} cm^{-2}. The protons had their end of range 50 μm below the surface in the highly doped substrate. The distribution of generated defects is expected to be nearly uniform in the active DLTS region (1–5 μm from the surface). Irradiation with 15 MeV electrons was performed at the Alfvén Laboratory in Stockholm. Annealings were performed under a flow of N_2 gas and, as no bias was applied, the monitored M centers were in configuration B during annealing.

A refined version of a constant-voltage DLTS setup described elsewhere[19] was employed for the capacitance measurements. The temperature range used was 77 to 350 K and for the DLTS measurements, rate windows ranged from (100 ms)$^{-1}$ to (3200 ms)$^{-1}$. Depth profiling and carrier capture coefficient measurements on individual defects were performed by fixing the sample temperature at the position of the appropriate DLTS peak. In the depth profiling measurements, the steady-state reverse bias voltage was kept constant, while the DLTS signal was measured as the amplitude of the majority-carrier pulse was gradually increased. To study charge carrier capture, the DLTS signal versus filling pulse durations was measured, making it possible to deduce the carrier capture cross section directly.

If the defect concentrations are small compared to the doping concentration, the DLTS peak heights are proportional to the defect concentrations. If independent peaks are overlapping, the total DLTS signal is given by the sum of the individual peaks. This means that DLTS spectra recorded on the same sample and with the same parameters can be subtracted to reveal the DLTS signature of the defect(s) responsible for any change in the spectra caused by, e.g., an additional annealing step or a change in configuration. Since we have investigated high-quality diodes enabling measurements with a high degree of reproducibility, we could make extensive use of subtracted spectra. This has proven to be a powerful tool when dealing with the complex DLTS spectra which are recorded after low annealing temperatures.

During so-called pulse-train measurements[15,20] the applied bias is repeatedly changed between two levels, filling and measurements bias. During the short (50 or 300 ns) filling pulses, empty defects start to capture majority carriers. The reverse bias capacitance is measured between the pulses, and here the defects may emit carriers again. After a sufficient number of such short pulses, steady state between capture and emission is established and the charge carrier population of defects saturates at a level that depends on temperature, filling pulse duration, and repetition frequency. In our case, the initial occupation of the defects was controlled by bias and temperature, and the response of the M center levels was revealed by subtracting pulse-train measurements from the configurations A and B. For each defect, the capture and emission process was controlled by the capture and emission rates, but also by the filling pulse duration t_p and time between pulses (1.75 s). The reverse-bias capacitance is measured 50 ms after the pulse.

III. RESULTS

A. The M center in 4H-SiC

After annealing at 200 °C, the upper part of the band gap is dominated by the Z, M, and S levels, as can be seen in Fig. 1 for a proton-implanted sample. Spectra from an unimplanted reference sample is shown together with DLTS spectra for configurations A and B of the M center. In the latter cases, all M centers were either completely in configuration A or completely in configuration B. It is seen that the M_1 and M_2 levels overlap with the S_1 and Z levels, respectively, but because of the opportunity to switch completely between configurations A and B, information on the M center levels can still be obtained, despite this overlap. There is also a partial overlap between M_3 and S_2, as seen in Fig. 1. The M center levels can be clearly revealed by subtracting DLTS measurements which vary only in the configuration of the M center. Subtracting the two DLTS spectra for configurations A and B in Fig. 1 results in the three DLTS peaks for M_1, M_2, and M_3 shown in Fig. 2. By combining such subtracted DLTS spectra with Arrhenius plots and simultaneous

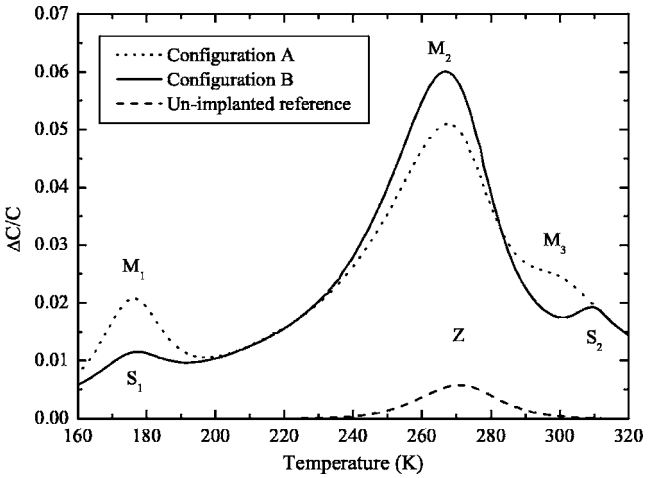

FIG. 1. DLTS temperature scan of 2.5 MeV proton-implanted 4H-SiC after annealing at 200 °C. The solid (dotted) curve was measured when all M centers were in configuration A (B). The DLTS spectrum for an unimplanted reference sample is shown for comparison. Rate window was (3.2 s)$^{-1}$.

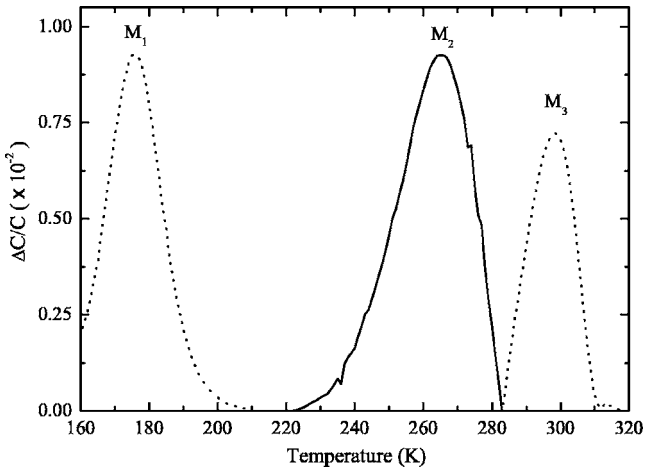

FIG. 2. DLTS signal for the three M center levels M_1, M_2, and M_3, obtained by subtracting configuration A and configuration B spectra. The results shown here are based on the DLTS spectra in Fig. 1. Rate window was (3.2 s)$^{-1}$.

TABLE I. Apparent energy position below the conduction-band edge and carrier capture cross section σ for M_1, M_2, and M_3. The σ_∞ values are extracted from Arrhenius plots whereas σ_{meas} refers to direct measurements. Direct measurements have been made at the indicated temperatures.

Defect level	Energy (eV)	σ_∞ ($\times 10^{-15}$ cm^2)	σ_{meas} ($\times 10^{-15}$ cm^2)	Temperature (K)
M_1	0.42	6	0.04–0.07	176, 187
M_2	0.63	4	0.02–0.06	244, 265, 281
M_3	~0.83	~300	>2	276

curve fitting of all the DLTS rate windows,[21] the apparent energy positions in the band gap and extrapolated carrier capture cross sections for the M center levels were extracted with a high accuracy. The results are shown in Table I.

Figure 3 depicts the defect concentration versus depth measured with a rate window of $(400\ \text{ms})^{-1}$ at 185.5 K. With these parameters, the total concentration of the overlapping M_1 and S_1 peaks is measured. In the figure, depth profiles are reported for three cases of M center configuration. In the first case, all M centers in the active DLTS region were in configuration A, while in the second case they were in configuration B. In the third case, only a low reverse bias was applied during reconfiguration heat treatment (50 °C) so that the edge of the depletion region was at ~2.8 μm, yielding the A configuration below ~2.8 μm and the B configuration at larger depths.

B. Annealing behavior

Both isochronal and isothermal annealing series have been performed. After each annealing, two DLTS spectra

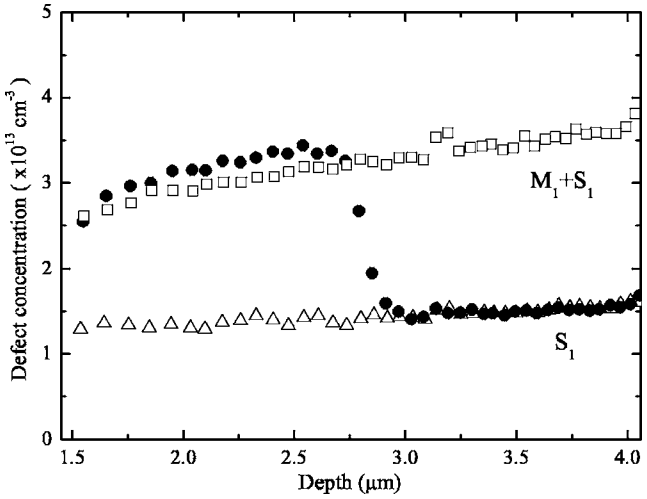

FIG. 3. Defect concentration versus depth for the overlapping defect levels M_1 and S_1. Depth profiles were measured when all M centers were in configuration B and only the overlapping S_1 signal was measured (triangles), when only half of the active DLTS region was depleted during reconfiguration heat treatment (circles), and when all M centers in the active region had been allowed to reconfigure from B to A (squares). Measurement temperature was 185.5 K and the rate window was $(400\ \text{ms})^{-1}$. The implantation fluence was 1×10^{12} cm^{-2}.

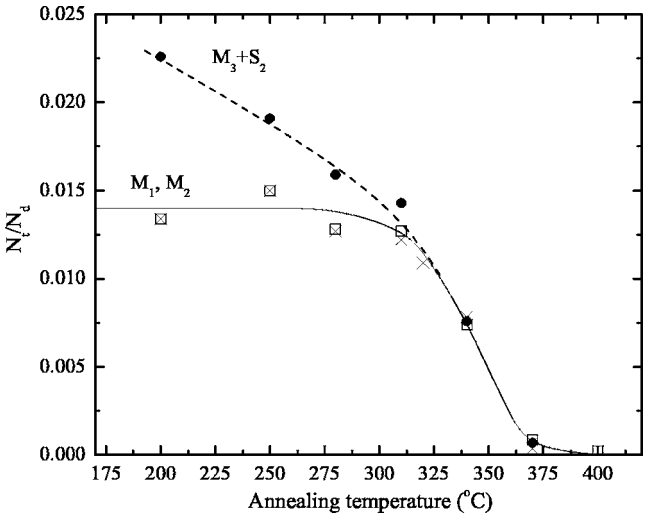

FIG. 4. Isochronal annealing (30 min). Concentration of M_1, M_2, and the sum of M_3 and S_2 as a function of annealing temperature. The concentrations of M_1 and M_2 are deduced from the height of their DLTS peaks in subtracted spectra like the one shown in Fig. 2. The concentration is expressed as the relation between the trap concentration N_t and the background doping N_d. The (M_3+S_2) concentration was found by comparing the configuration A DLTS spectrum at each annealing temperature to the spectrum at 400 °C. Lines are included to guide the eye.

were measured. The annealing itself, during which no bias was applied, placed all monitored M centers in configuration B. This configuration was measured by scanning the temperature from 275 to 77 and back to 320 K. During the final part of the measurement (285–320 K) the M centers gradually changed to configuration A (as described in Ref. 11). To assure a complete transformation, the bias was applied at 320 K for at least 5 min before the second DLTS spectrum (configuration A) was recorded. The concentrations of M_1 and M_2 in Figs. 4 and 5 were found from the DLTS peak heights in the subtracted spectrum. The results from the

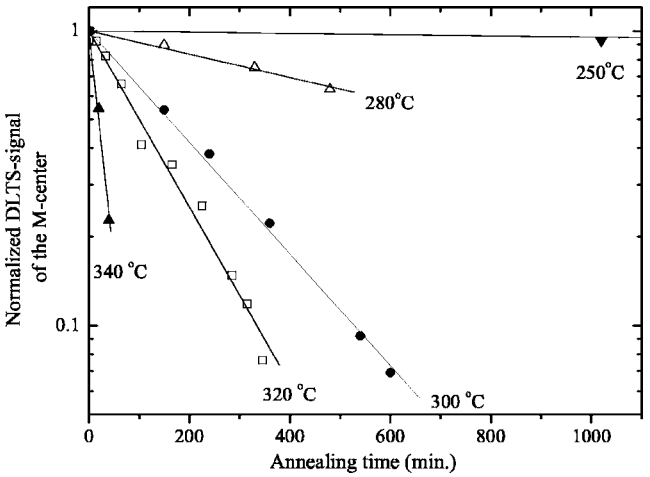

FIG. 5. Isothermal annealing. Normalized M center concentration as a function of annealing time at 250, 280, 300, 320, and 340 °C. Determination of the rate of annealing at 250 °C is based on four points, of which only the first one is shown.

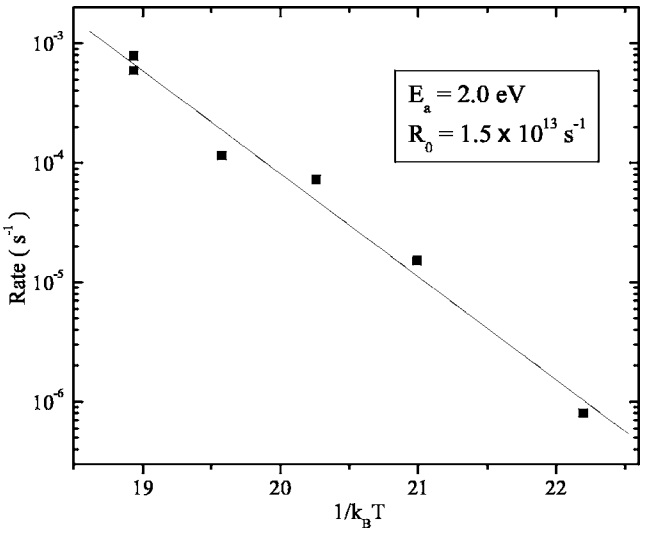

FIG. 6. Rate of M center annealing versus $1/k_BT$. The Arrhenius plot gives an activation energy of 2.0 eV and a prefactor of 1.5×10^{13} s^{-1}. Five of the measured points come from the five isothermal annealings shown in Fig. 5, and the sixth point (at 340 °C) is extracted from the isochronal annealing data.

30 min isochronal annealing series on the same sample are shown in Fig. 4. The concentration of M_3 could not be found by subtraction due to the gradual transformation at 285–320 K, but the total concentration of M_3 and S_2 could be found by following the development in the configuration A spectra.

The results of the isothermal annealings series are shown in Fig. 5 for five different temperatures, and first-order kinetics (exponential decay) is found. The annealing rates at these five temperatures (indicated by lines in Fig. 5 and determined by least-squares fits) are shown in Fig. 6 as a function of $1/k_BT$, where k_B is Boltzmann's constant and T is the absolute annealing temperature. The additional point at 340 °C was extracted from the isochronal annealing series (Fig. 4) and agrees very well with the isothermal points. The annealing rate R can be described by

$$R(T) = R_0 \exp\left(\frac{-E_a}{k_BT}\right), \tag{1}$$

where E_a is the activation energy of the process and R_0 is a prefactor. A linear fit of the six points plotted in the semilogarithmic Arrhenius graph (Fig. 6) gives $E_a = 2.0$ eV and a prefactor of $R_0 = 1.5 \times 10^{13}$ s^{-1}. Notice that the measured annealing rates span three orders of magnitude.

C. Capture and emission of charge carriers

The reverse-bias capacitance is always recorded concurrently with the DLTS signal as a function of temperature. A careful comparison between such reverse bias capacitance curves for the configurations A and B is shown in Fig. 7. At low (<180 K) and high (>305 K) temperatures the two curves overlap perfectly, but in between these temperatures the capacitance is higher if the M centers are in configuration A. The difference in capacitance is about 1 pF and remains

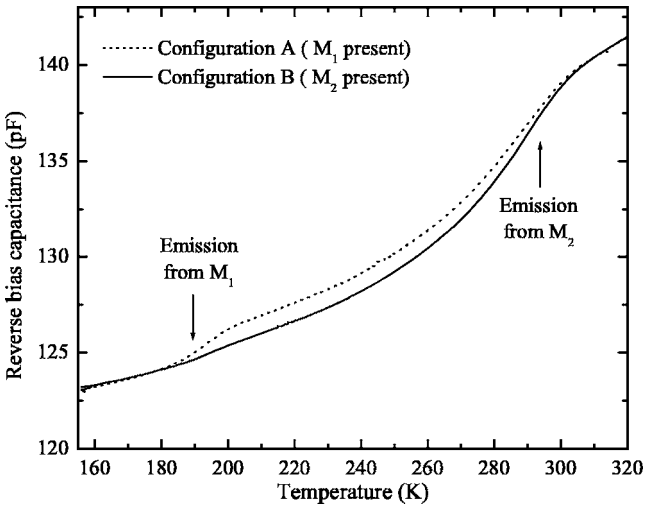

FIG. 7. Reverse-bias capacitance as a function of temperature after annealing at 300 °C. Curves from configurations A and B are shown, and a difference of about 1 pF can be seen between 200 and 275 K.

constant between 200 and 275 K. The splitting of the two curves (at ~180–200 K) coincides with the temperature for the M_1 emission of electrons, and the rejoining (at ~275–305 K) coincides with the M_2 emission of electrons.

To measure the charge carrier capture cross section directly, the DLTS signal was measured as a function of filling pulse duration for M_1, M_2, and M_3. This was done in both configurations and the filling pulse curves for the three levels were deduced by subtraction. The filling pulse curves for M_2 measured at 265 K with a reverse bias of 5 and 15 V are shown in Fig. 8. A theoretical expression for the filling pulse curve of a uniformly distributed deep level with a concentration well below the doping concentration is given by Pons.[22] Fitting the experimental data in Fig. 8 with this expression

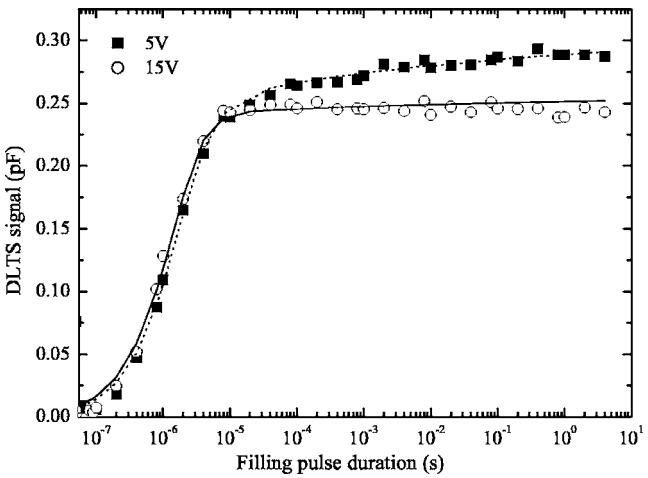

FIG. 8. The filling kinetics for M_2 obtained from subtracted DLTS signal versus filling pulse duration measurements after annealing at 200 °C. Results are shown for reverse biases of 5 and 15 V together with calculated curves according to Pons (Ref. 22). The rate window used was $(3200 \text{ ms})^{-1}$ and the measurement temperature was 265 K.

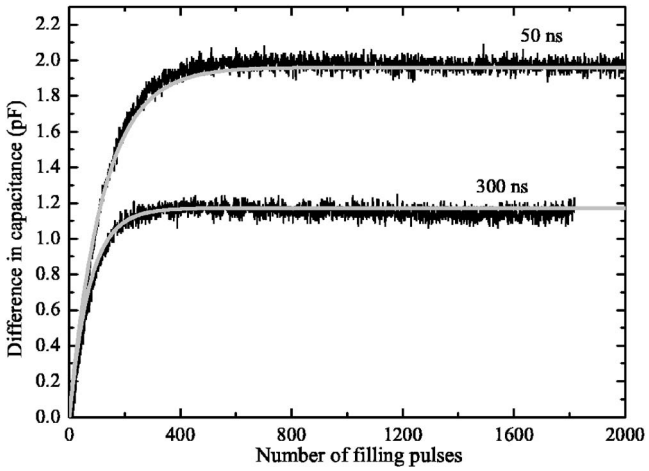

FIG. 9. Difference in reverse-bias capacitance during pulse-train measurements versus number of applied filling pulses. The difference is between identical measurements on configurations *A* and *B*. The sample temperature was 150 K [procedure (i)]. The solid line represents simulation results.

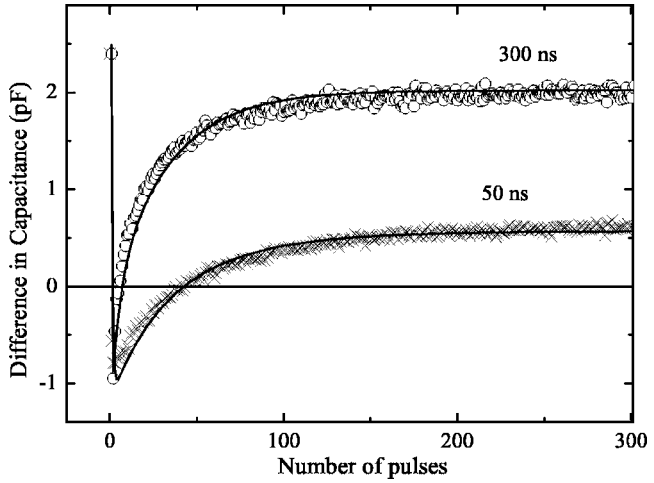

FIG. 10. Difference in reverse-bias capacitance during pulse-train measurements versus number of applied filling pulses. The difference is between identical measurements on configurations *A* and *B*. Defect levels were emptied at 275 K and kept empty until the pulse-train measurements were started at 220 K [procedure (iv)]. The first point is measured before the first pulse is applied. The solid line represents simulation results.

gives a capture cross section of 4.7×10^{-17} cm^2 (5 V) and 5.3×10^{-17} cm^2 (15 V) for M_2 at 265 K. The results from all the measurements of the capture cross sections are summarized in Table I.

Pulse-train measurements have been performed with four different initial occupation of the defects: (i) stabilizing the temperature at 150 K, long initial filling pulse (>30 s), and then a pulse-train measurement with a certain filling pulse duration, (ii) as in (i) but at 220 K, (iii) stabilizing the temperature at 220 K, long initial filling pulse followed by an emptying under reverse bias for 120 s, cooling to 150 K with reverse bias, and then a pulse-train measurement, and (iv) as in (iii) but emptying at 275 K and measurement at 220 K. For each case, pulse-train measurements were performed with different pulse durations. The results for (i) are shown in Fig. 9 for filling pulse durations of 50 and 300 ns, along with simulation results which are discussed below. Again, we stress that it is the difference between two pulse-train measurements (*A* and *B*), that is shown in Fig. 9, and because of this, only the effect of the *M* center levels is displayed. The corresponding experimental and simulation results for (iv) are shown in Fig. 10. The pulse-train measurements were performed on *M* centers generated by 15 MeV electron irradiation.

IV. DISCUSSION

A. Depth profile of the *M* center

In the investigated region, the defects are expected to be almost uniformly distributed, but Fig. 3 shows a gradual increase with depth for both the *S* and *M* centers. The increase is not an artifact caused by, for instance, a nonuniform doping concentration. Instead, the increase can be linked to the depth distribution of the primary irradiation damage as calculated by TRIM (Ref. 23) and it is less likely to be caused by either surface-point defect interactions,[24] or the involvement of a nonuniformly distributed impurity in the *M* center. The identity of the *M* center is not yet known and the use of complementary characterization techniques is needed. As the *M* center is introduced by both electron and proton irradiation, the implanted hydrogen atoms are not involved in the defect. Any correlation with residual impurity hydrogen cannot, however, be excluded.

B. Annealing behavior

According to the isochronal annealings (Fig. 4), M_1 and M_2 display identical behavior, and M_3 is considered to be similarly affected by the annealings, as the sum of M_3 and S_2 disappears together with M_1 and M_2 between 310 and 400 °C. The decrease in the total concentration of M_3 and S_2 below 310 °C corresponds well with the annealing of S_1 in our samples and with the annealing of the *S* defect reported in Ref. 10. In the subtracted spectra (Fig. 2), the M_3 peak appears lower than the M_1 and M_2 peaks due to the gradual reconfiguration process[11] which takes place between 285 and 320 K. We conclude that the *M* center anneals out between 310 and 370 °C and Fig. 4 strongly supports the assignment of the three levels M_1, M_2, and M_3 to the same defect.

The isothermal annealing results show that the *M*-center loss displays first-order kinetics over more than one order of magnitude in defect concentration (300 and 320 °C in Fig. 5). This first-order behavior can be explained by three different mechanisms: (i) defect dissociation, (ii) *M* center migration followed by trapping at another, significantly more abundant defect, or (iii) interaction between a mobile, abundant defect and an immobile *M* center. The prefactor for the thermally activated process was found to be $\sim1.5\times10^{13}$ s^{-1} (Fig. 6) which is, within the experimental accuracy, identical to a theoretical estimate[25] of the lattice vibration frequency in 4*H*-SiC at 300 °C, $\sim1.6\times10^{13}$ s^{-1}. Hence,

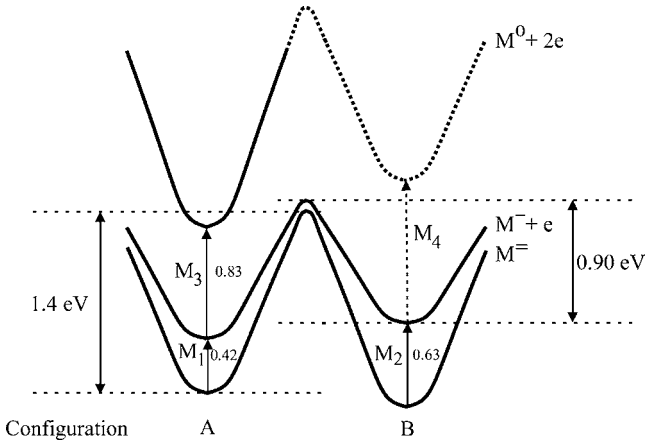

FIG. 11. Suggested configuration diagram for the *M* center in 4*H*-SiC.

this strongly favors a pure dissociation process with negligible back reaction (association). For mechanisms (ii) and (iii), which involve defect or impurity migration, substantially lower prefactors are anticipated, typically $\leqslant 10^{10}$ s^{-1} assuming a trap concentration of $\leqslant 10^{16}$ cm^{-3} and diffusion prefactor of $\leqslant 1$ cm^2/s. Thus, (ii) and (iii) are ruled out as the main annealing mechanisms for the *M* center, and dissociation dominates.

The temperature range of annealing is similar to what Itoh *et al.*[26] reported for the intrinsic *T*6 and *T*7 defects in 3*C*-SiC. These defects have, however, only been seen in *p*-type material and no metastability has yet been reported. The identity of the *M* center is still unresolved.

C. Charge states and configuration diagram

In Fig. 11, a configuration diagram for the *M* center is suggested. The diagram is consistent with all our results, as discussed in the following. The M_1 and M_2 levels are assigned to the same charge state transition for two reasons. First, at temperatures below 180 K both M_1 and M_2 are filled and the total amount of charge in the depletion region is the same, irrespectively of the *M* center configuration (see Fig. 7). Figure 7 also shows that the total amount of (positive) charge in the depletion region is increased (seen by the increase in reverse-bias capacitance) when M_1 and M_2 emit their trapped electrons in configurations *A* and *B*, respectively. The splitting between the two capacitance curves in Fig. 7 occurs because M_1 ($E_C-0.42$ eV) is shallower than M_2 ($E_C-0.63$ eV). This means that M_1 is empty and M_2 filled between 200 and 275 K. It should be mentioned that the rejoining of the capacitance curves at 275–305 K is assisted by the gradual transition from configuration *B* to *A*, but it cannot be explained by the reconfiguration alone. Second, the direct measurements on M_1 and M_2 revealed very similar carrier capture cross sections and this indicates that M_1 and M_2 belong to transitions between the same charge states. Indications of the absolute charge states can be deduced from the measured carrier capture cross section values. The values for M_1 and M_2 ($\sigma \approx 5\times 10^{-17}$ cm^2) suggest a (=/−) transition. Further, because no peaks are observed between M_1 and M_3 in configuration *A* and because the DLTS peak amplitudes of M_1 and M_3 are the same, M_3 is assigned to a (−/0) transition. This is also consistent with the higher capture cross section ($>2\times 10^{-15}$ cm^2) for M_3.

It should be mentioned that no Poole-Frenkel effect has been observed for M_1 and M_2—indicating acceptor-type levels, but the absence of such an effect cannot be used to conclude strongly on the charge state of a defect.[27]

Table I shows that the carrier capture cross sections extracted from the Arrhenius plot using T^2 corrections are much larger than the measured ones for M_1 and M_2. This discrepancy is normally attributed to a large change in entropy, ΔS for the defect as it emits the electron.[28] Assuming that the capture cross sections are independent of temperature, ΔS becomes approximately $5k_B$ for M_1 and for M_2.

Compelling evidence for the existence of a second level, labeled M_4, for configuration *B* is provided by Fig. 7. Below ~180 K, where both M_1 and M_3 are filled, configurations *A* and *B* display the same capacitance values showing that the two configurations accommodate the same amount of charge. That is, for configuration *B*, the M_2 level is not sufficient but one additional state must exist, and it is deeper than M_2 since the two capacitance curves merge above ~295 K where M_2 is empty and M_3 still (partly) populated. This is also consistent with the observations that the merge of the curves cannot be accounted for only by the reconfiguration from *B* to *A*. Further evidence for the fourth charge state will be discussed below.

Reconfiguration from *B* to *A* has a barrier of 0.9 eV and takes place when M_2 is empty—hence the placement of the 0.9 eV barrier in Fig. 11. It should be pointed out that thermal carrier emission from M_2 is not the limiting factor when it comes to the transition from $B^=$ to B^- to A^-. At 300 K, the first process takes place on a subsecond time scale whereas the reconfiguration process has a time scale of several minutes. It may look striking that M_3 emission and *B* to *A* reconfiguration have similar activation energies, but the two processes are uncorrelated as the change is *from B to A* and the time scale for M_3 emission is on the order of a few seconds at 300 K.

When the reconfiguration barrier for the transformation from *A* to *B* was determined[11] to 1.4 eV, the temperatures and samples used were such that both M_1 and M_2 were filled, i.e., below the Fermi level. This gives the 1.4 eV barrier between $A^=$ and $B^=$ in Fig. 11.

D. Simulations of reverse-bias capacitance during filling pulse train measurements

The simulations of the pulse-train measurements are based on a model where the difference in reverse bias capacitance is given by

$$\Delta C_{rev} \approx \text{const} \times (Q_A - Q_B) \tag{2}$$

assuming that all other defects are unaffected by the configuration of the *M* center, and also that the concentration of defects is low compared to the doping concentration. Q_A and Q_B are the charges from the *M* centers contributing to the depletion region capacitance, in configurations *A* and *B*, re-

spectively. Three charge states (=/−/0) are considered for both configurations and it is assumed that the sum of the corresponding three occupation fractions f is unity. The transition $B^- \leftrightarrow B^0$ has not been explicitly observed experimentally, but it is included in the model due to the discussion about M_4 that followed Fig. 7. Capture and emission rates for the levels M_1, M_2, M_3, and M_4 are used as input parameters in the simulations. Measurements undertaken at 150 K [case (i), initially filled levels] are shown in Fig. 9. When the M centers are all in configuration B, the M_2 (and M_4) levels are all filled because the emission rate for M_2 is extremely low at 150 K (see Fig. 2). In configuration A, the M_1 (and M_3) levels are also filled initially, but the emission rate is not negligible so the M_1 defects will partly fill during each pulse and partly empty during each measurement interval, until steady-state conditions are established. Figure 9 shows that in the beginning, where defects in either configuration of the M center are filled, $\Delta C_{rev} \approx 0$, and M_1 and M_2 must therefore be transitions between the same charge states. As the occupation fraction $f(A^=)$ drops from 1 toward its steady-state value, then ΔC_{rev} increases and even more so for shorter filling pulses (50 versus 300 ns). The experimental data in Fig. 9 were reproduced by an emission rate of 0.004 s^{-1} and a capture rate of 2×10^4 s^{-1}; these values are close to those expected from an extrapolation of the DLTS results for M_1.

In fact, using reasonable input parameters, the model could account for all the experimental observations using different initial filling conditions [(i) to (iv)]. This was impossible if M_1 and M_2 were assigned to different charge state transitions. Absolute charge states of =/−/0 were assumed but using charge states of −/0/+ would yield identical simulation results. As discussed earlier, however, the direct measurements of the capture cross sections favor (=/−) and (−/0) for M_1 and M_3, respectively.

Finally, it should be emphasized that also the simulations strongly support the existence of a single acceptor state M_4 for configuration B. In Fig. 10, ΔC_{rev} is positive *before* the first filling pulse, but substantially negative *after* the first pulse. This is attributed to partial emptying of the single negative charge state in configuration B (M_4) and almost complete emptying in configuration A (M_3) at 275 K, with a rapid capture for M_3 at 220 K. Further, the capture rate for M_4 was much larger than that of M_2, consistent with assigning M_4 to a (−/0) transition, while the emission rate for M_4 was somewhat lower than that of M_3. This places the M_4 level inside the band gap at a position deeper, but not much deeper, than M_3. Hence, M_4 escapes detection by DLTS as the M center changes configuration from B to A (at ~300 K) before the temperatures needed to observe M_4 are reached.

V. CONCLUSIONS

The irradiation-induced, metastable M defect in 4H-SiC has been studied in detail. Three levels M_1, M_2, and M_3 are directly observed in DLTS measurements and compelling indirect evidence is obtained for a fourth level M_4, located deeper in the band gap than M_3. On the basis of an extensive set of experimental data (DLTS, capacitance versus temperature, pulse-train measurements) together with simulations of charge carrier capture and emission, a detailed configuration diagram for the M center is presented, where M_1 and M_3 correspond to a doubly and singly negative charge state of the M center in configuration A, while M_2 and M_4 correspond to a doubly and singly negative charge state in configuration B. The M center is observed to anneal out between 310 and 370 °C, with first-order kinetics and a rate given by $(1.5 \times 10^{13}\ s^{-1})[\exp(-2.0\ eV)/k_B T]$, strongly suggesting that dissociation is the main annealing mechanism.

ACKNOWLEDGMENTS

Assistance by Dr. Uwe Zimmermann for Schottky diode preparation is highly appreciated. Partial financial support was gratefully accepted from the Swedish Foundation for Strategic Research and from the Norwegian Research Council.

*Electronic address: hkn@imit.kth.se

[1] J. P. Doyle, M. K. Linnarsson, P. Pellegrino, N. Keskitalo, B. G. Svensson, A. Schöner, N. Nordell, and J. L. Lindström, J. Appl. Phys. **84**, 1354 (1998).
[2] P. Lévêque, D. Martin, B. G. Svensson, and A. Hallén, Mater. Sci. Forum **433-436**, 415 (2003).
[3] M. L. David, G. Alfieri, E. M. Monakhov, A. Hallén, C. Blanchard, B. G. Svensson, and J. F. Barbot, J. Appl. Phys. **95**, 4728 (2004).
[4] H. Kortegaard Nielsen, A. Hallén, D. M. Martin, and B. G. Svensson, Mater. Sci. Forum **483-485**, 497 (2005).
[5] A. A. Lebedev, A. M. Ivanov, and N. B. Strokan, Semiconductors **38**, 125 (2004).
[6] I. Pintilie, L. Pintilie, and K. Irmscher, Appl. Phys. Lett. **81**, 4841 (2002).
[7] T. A. G. Eberlein, R. Jones, and P. R. Briddon, Phys. Rev. Lett. **90**, 225502 (2003).
[8] L. Storasta, A. Henry, J. P. Bergman, and E. Janzén, Mater. Sci. Forum **457-460**, 469 (2004).
[9] D. Åberg, L. Storasta, A. Hallén, and B. G. Svensson, Mater. Sci. Forum **353-356**, 443 (2001).
[10] M. L. David, G. Alfieri, E. V. Monakhov, A. Hallén, J. F. Barbot, and B. G. Svensson, Mater. Sci. Forum **433-436**, 371 (2003).
[11] D. M. Martin, H. Kortegaard Nielsen, P. Lévêque, A. Hallén, G. Alfieri, and B. G. Svensson, Appl. Phys. Lett. **84**, 1704 (2004).
[12] G. E. Jellison, Jr., J. Appl. Phys. **53**, 5715 (1982).
[13] L. W. Song, X. D. Zhan, B. W. Benson, and G. D. Watkins, Phys. Rev. B **42**, 5765 (1990).
[14] X. D. Zhan and G. D. Watkins, Phys. Rev. B **47**, 6363 (1993).
[15] C. G. Hemmingsson, N. T. Son, O. Kordina, and E. Janzén, J. Appl. Phys. **91**, 1324 (2002).
[16] O. Kordina, C. Hallin, A. Henry, J. P. Bergman, I. Ivanov, A. Ellison, N. T. Son, and E. Janzén, Phys. Status Solidi B **202**, 321 (1997).

[17] S.-K. Lee, C.-M. Zetterling, and M. Östling, J. Appl. Phys. **87**, 8039 (2000).
[18] A. Hallén, P. A. Ingemarsson, P. Håkansson, and B. U. R. Sundqvist, Nucl. Instrum. Methods Phys. Res. B **36**, 345 (1989).
[19] B. G. Svensson, K.-H. Rydén, and B. M. S. Lewerentz, J. Appl. Phys. **66**, 1699 (1989).
[20] C. H. Henry, H. Kukimoto, G. L. Miller, and F. R. Merritt, Phys. Rev. B **7**, 2499 (1973).
[21] A. A. Istratov, H. Hieslmair, C. Flink, and E. R. Weber, Rev. Sci. Instrum. **69**, 244 (1998).
[22] D. Pons, J. Appl. Phys. **55**, 3644 (1984).
[23] J. P. Biersack and L. G. Haggmark, Nucl. Instrum. Methods **174**, 257 (1980).
[24] K. L. Wang, Y. H. Lee, and J. W. Corbett, Appl. Phys. Lett. **33**, 547 (1978).
[25] M. S. Janson, A. Hallén, M. K. Linnarsson, and B. G. Svensson, Phys. Rev. B **64**, 195202 (2001).
[26] H. Itoh, A. Kawasuso, T. Ohshima, M. Yoshikawa, I. Nashiyama, S. Tanigawa, S. Misawa, H. Okumura, and S. Yoshida, Phys. Status Solidi A **162**, 173 (1997).
[27] S. D. Ganichev, E. Ziemann, I. N. Yassievich, W. Prettl, A. A. Istratov, and E. R. Weber, Phys. Rev. B **61**, 10361 (2000).
[28] O. Engström and A. Alm, Solid-State Electron. **21**, 1571 (1978).